university of groningen

University Medical Center Groningen

University of Groningen

Investigation of nuclear forces in d + p elastic and p + d break-up reactions at intermediate energies

Mardanpour-Mollalar, Hossein

IMPORTANT NOTE: You are advised to consult the publisher's version (publisher's PDF) if you wish to cite from it. Please check the document version below.

Document Version
Publisher's PDF, also known as Version of record

Publication date:
2008

Link to publication in University of Groningen/UMCG research database

Citation for published version (APA):
Mardanpour-Mollalar, H. (2008). *Investigation of nuclear forces in d + p elastic and p + d break-up reactions at intermediate energies.* s.n.

Copyright
Other than for strictly personal use, it is not permitted to download or to forward/distribute the text or part of it without the consent of the author(s) and/or copyright holder(s), unless the work is under an open content license (like Creative Commons).

The publication may also be distributed here under the terms of Article 25fa of the Dutch Copyright Act, indicated by the "Taverne" license. More information can be found on the University of Groningen website: https://www.rug.nl/library/open-access/self-archiving-pure/taverne-amendment.

Take-down policy
If you believe that this document breaches copyright please contact us providing details, and we will remove access to the work immediately and investigate your claim.

Downloaded from the University of Groningen/UMCG research database (Pure): http://www.rug.nl/research/portal. For technical reasons the number of authors shown on this cover page is limited to 10 maximum.

Download date: 05-05-2023

A. The interaction of particles with spin with an external magnetic field

A.1 Description of the polarization

In this section the general spin formalism for a vector-polarized proton and a tensor-polarized deuteron beam is described. In the following, we follow the formalism as presented in Ref. [54].

A.1.1 Spin-$\frac{1}{2}$ particles

The spin state of a particle with spin $\frac{1}{2}$ can be represented by a Pauli spinor,

$$\chi = \begin{pmatrix} a_1 \\ a_2 \end{pmatrix}. \tag{A.1}$$

The expectation value of an observable such as Ω is:

$$< \Omega >= \chi^{\dagger}\Omega\chi \equiv |a_1|^2\Omega_{11} + |a_2|^2\Omega_{22} + 2Re\Omega_{12}a_1^*a_2. \tag{A.2}$$

It is convenient to define the density matrix ρ such that: $< \Omega >=\mathrm{Tr}\rho\Omega$, where

$$\rho = \begin{pmatrix} |a_1|^2 & a_1a_2^* \\ a_2a_1^* & |a_2|^2 \end{pmatrix}. \tag{A.3}$$

The polarization state of a spin-$\frac{1}{2}$ particle is specified by the Pauli spin operators σ_x, σ_y and σ_z:

$$\sigma_x = 2S_x = \begin{pmatrix} 0 & 1 \\ 1 & 0 \end{pmatrix}, \ \sigma_y = 2S_y = \begin{pmatrix} 0 & -i \\ i & 0 \end{pmatrix}, \ \sigma_z = 2S_z = \begin{pmatrix} 1 & 0 \\ 0 & -1 \end{pmatrix}, \tag{A.4}$$

where the Pauli matrices obey the following commutation rules:

$$[\sigma_i, \sigma_j] = 2i\epsilon_{ijk}\sigma_k \tag{A.5}$$

and $Tr(\sigma_i\sigma_j) = 2\delta_{ij}$. The spin-$\frac{1}{2}$ density matrix, ρ, can be expanded in terms of the set of matrices, I, σ_x, σ_y and σ_z, since these operators form a complete set of hermitian matrices for the 2×2 space,

$$\rho = \frac{1}{2}(I + p_x\sigma_x + p_y\sigma_y + p_z\sigma_z). \tag{A.6}$$

For a polarized proton beam with spinors $\begin{pmatrix}\sqrt{N^{\uparrow}}\\ \sqrt{N^{\downarrow}}\end{pmatrix}$ the probability of finding p_z is:

$$p_z =< \sigma_z >= Tr(\rho\sigma_z) = \frac{N^{\uparrow} - N^{\downarrow}}{N^{\uparrow} + N^{\downarrow}}. \tag{A.7}$$

A beam of spin-$\frac{1}{2}$ particles can be uniquely characterized by its vector polarization, p_z, defined as Eq. A.7.

A.1.2 Spin-1 particles

A spin-1 particle is characterized by a three-component spinor:

$$\chi = \begin{pmatrix} a_1 \\ a_2 \\ a_3 \end{pmatrix}.$$

The basic spin-1 angular momentum operators are:

$$S_x = \frac{1}{\sqrt{2}}\begin{pmatrix}0&1&0\\1&0&1\\0&1&0\end{pmatrix},\ S_y = \tfrac{1}{\sqrt{2}}\begin{pmatrix}0&-i&0\\i&0&-i\\0&i&0\end{pmatrix},\ S_z = \begin{pmatrix}1&0&0\\0&0&0\\0&0&-1\end{pmatrix}. \tag{A.8}$$

These operators together with the unitary matrix, $I(3\times 3)$, and 6 other tensor operators spans 3×3 space. The tensor operators are:

$$\mathcal{P}_{xy} = \frac{3}{2}(S_xS_y + S_yS_x) = \frac{3i}{2}\begin{pmatrix}0&0&-1\\0&0&0\\1&0&0\end{pmatrix};\ \mathcal{P}_{yz} = \tfrac{3}{2}(S_yS_z + S_zS_y) = \tfrac{3i}{\sqrt{8}}\begin{pmatrix}0&-1&0\\1&0&1\\0&-1&0\end{pmatrix};$$
$$\mathcal{P}_{xz} = \frac{3}{2}(S_xS_z + S_zS_x) = \frac{3}{\sqrt{8}}\begin{pmatrix}0&1&0\\1&0&-1\\0&-1&0\end{pmatrix};\quad \mathcal{P}_{xx} = 3S_xS_x - 2I = \tfrac{1}{2}\begin{pmatrix}-1&0&3\\0&2&0\\3&0&-1\end{pmatrix};$$
$$\mathcal{P}_{yy} = 3S_yS_y - 2I = \frac{1}{2}\begin{pmatrix}-1&0&-3\\0&2&0\\-3&0&-1\end{pmatrix};\qquad \mathcal{P}_{zz} = 3S_zS_z - 2I = \begin{pmatrix}1&0&0\\0&-2&0\\0&0&1\end{pmatrix}. \tag{A.9}$$

These 10 operates, 6 tensor operators together with $I(3\times 3)$ and 3 vector operators, span the 3×3 space; however, only nine are needed. By using the following relation between the $\mathcal{P}_{ii}$ quantities:

$$\mathcal{P}_{xx} + \mathcal{P}_{yy} + \mathcal{P}_{zz} = 0 \tag{A.10}$$

we can eliminate one of 10 operators by using Eq. A.10 and are left with 9 operators.

It can be shown that the expectation value of these quantities are limited to ± 1 for the vector quantities, $\pm\frac{3}{2}$ for the $\mathcal{P}_{ij}$ quantities, and $+1$ and -2 for the $\mathcal{P}_{ii}$ quantities.

The density matrix can, therefore, be expanded in terms of these operators as follows:

$$\rho = \frac{1}{3}[I + \frac{3}{2}(p_x\mathcal{P}_x + p_y\mathcal{P}_y + p_z\mathcal{P}_z) + \frac{2}{3}(p_{xy}\mathcal{P}_{xy} + p_{yz}\mathcal{P}_{yz} + p_{xz}\mathcal{P}_{xz}) + \frac{1}{6}(p_{xx} - p_{yy})(\mathcal{P}_{xx} - \mathcal{P}_{yy}) + \frac{1}{2}p_{zz}\mathcal{P}_{zz}]. \tag{A.11}$$

Consider, for example, a beam of particles prepared by a system (such as a polarized ion source) with axial symmetry along the z axis. The most general form for the density matrix will then be:

$$\rho = \frac{1}{3}(I + \frac{3}{2}p_z\mathcal{P}_z + \frac{1}{2}p_{zz}\mathcal{P}_{zz}). \tag{A.12}$$

For a polarized spin-1 particle with spinor,

$$\begin{pmatrix} \sqrt{N^\uparrow} \\ \sqrt{N^0} \\ \sqrt{N^\downarrow} \end{pmatrix}, \tag{A.13}$$

the expectation value for p_z, and p_{zz} are:

$$p_z = \frac{N^\uparrow - N^\downarrow}{N^\uparrow + N^0 + N^\downarrow}, \quad p_{zz} = \frac{N^\uparrow - 2N^0 + N^\downarrow}{N^\uparrow + N^0 + N^\downarrow} = 1 - \frac{3N^0}{N^\uparrow + N^0 + N^\downarrow}. \tag{A.14}$$

where p_z and p_{zz} are the vector and tensor polarization values, respectively.

A.2 Hyperfine structure of the hydrogen atom

The hyperfine structure comes from the interaction of the proton dipole moment $\vec{\mu_p}$ with both the spin dipole moment of the electron $\vec{\mu_e}$ and the orbital dipole moment of the electron $\vec{L}$. Like the electron, the proton has spin angular momentum with s=1/2, and associated with this angular momentum, there is an intrinsic dipole moment:

$$\vec{\mu}_p = \gamma_p \frac{e}{M_p c}\vec{S}_p, \tag{A.15}$$

where M_p is the proton mass, $\gamma_p = 2.7928$ is the proton gyromagnetic ratio, and e, c are the electron charge and speed of light, respectively [79]. Note that the proton dipole moment is weaker than the electron dipole moment by roughly a factor of $M_p/m_e \sim 2000$, and hence one expects the associated effects to be smaller, in comparison to fine structure. Treating the corrections as a perturbation is, therefore, justified. As mentioned above, the proton dipole moment will interact with both the spin dipole moment of the electron and the orbital dipole moment of the electron, and so there are two new contributions to the Hamiltonian, the spin-orbit, $\vec{L}\cdot\vec{S}_p$, interaction and the spin-spin, $\vec{S}_p\cdot\vec{S}_e$, interaction. The derivation for the nuclear spin-orbit Hamiltonian is the same as for the electron spin-orbit Hamiltonian. The nuclear spin-orbit Hamiltonian is:

$$\Delta H_{so} = \frac{\gamma_p e^2}{m_e M_p c^2 r^3}\vec{L}\cdot\vec{S}_p. \tag{A.16}$$

The spin-spin Hamiltonian can be derived by considering the field produced by the proton spin dipole, which can be written as:

$$\vec{B}(\vec{r}) = \frac{1}{\vec{r^3}}[3\frac{(\vec{\mu}_p.\vec{r})\cdot\vec{r}}{r^2} - \vec{\mu}_p] + \frac{8\pi}{3}\vec{\mu}_p\delta^3(\vec{r}) \tag{A.17}$$

$$\Delta E_{ss} = -\vec{\mu}_e\cdot\vec{B}(\vec{r}) = \frac{\gamma_p e^2}{m_e M_p c^2}[\frac{1}{r^3}(3(\vec{S}_p\cdot\hat{r})(\vec{S}_e\cdot\hat{r}) - (\vec{S}_p\cdot\vec{S}_e)) + \frac{8\pi}{3}(\vec{S}_p\cdot\vec{S}_e)\delta^3(r)].$$

The total angular momentum can be written as:

$$\vec{F} = \vec{L} + \vec{S}_e + \vec{S}_p = \vec{J} + \vec{S}_p. \tag{A.18}$$

The corresponding operators F^2 and F_z commute with the Hamiltonian, and they introduce new quantum numbers, F, and m_F. The quantum number F has possible values $F = j+1/2, j-1/2$ since the proton has spin $1/2$. Therefore, every energy level associated with a particular set of quantum numbers n, l, and j will be split into two levels with a slightly different energies, depending on the relative orientation of the proton spin with respect to the electron spin.

Since the hyperfine splitting of the ground state of hydrogen atom is of particular interest here, we consider first the case $l = 0$. Since the electron has no orbital angular momentum, there is no spin-orbit effect. It can be shown that because the wave function has spherical symmetry, only the delta function term from the spin-spin Hamiltonian contributes. First-order perturbation theory yields then:

$$\Delta E_{hfs} = \frac{8\pi\gamma_p e^2}{3m_e M_p c^2}(\vec{S}_e\cdot\vec{S}_p)|\psi(0)|^2. \tag{A.19}$$

where ΔE_{hfs} is the first-order energy perturbation from the hyperfine structure effect. The value of $S_e\cdot S_p$ can be found by squaring F, which for $l = 0$ gives,

$$\vec{S}_e\cdot\vec{S}_p = \frac{1}{2}[F^2 - S_e^2 - S_p^2]. \tag{A.20}$$

Hence,

$$\vec{S}_e\cdot\vec{S}_p = \frac{\hbar^2}{2}[F(F+1) - s_p(s_p+1) - s_e(s_e+1)] = \frac{\hbar^2}{2}[F(F+1) - \frac{3}{2}],$$

where in the last step, the values $s_e = s_p = 1/2$ are used. The hyperfine energy shift for $l = 0$ is then:

$$\Delta E_{hfs} = A[F(F+1) - \frac{3}{2}], \quad A = (\frac{4}{3}\frac{m_e}{M_p}\alpha^4 m_e c^2\frac{\gamma_p}{n^3}), \tag{A.21}$$

where n is the orbital quantum number of Hydrogen, and $\alpha = \frac{1}{137}$ is the fine structure constant. It is easy to see from this expression that the hyperfine splittings are smaller than the fine structure by a factor of M_p/m_e. For the specific case of the ground state of the hydrogen atom ($n = 1$), the energy separation between the states of $F = 1$ and $F = 0$

is:

$$\Delta E_{hfs}(F=1) - \Delta E_{hfs}(F=0) = 5.9 \times 10^{-6}\text{eV}. \tag{A.22}$$

The photon corresponding to the transition between these two states has a frequency of $\nu = 1.42$ GHz.

For atoms other than hydrogen, the nuclear spin I and the total electron angular momentum $\vec{J} = \vec{L} + \vec{S}$ are coupled, giving rise to the total angular momentum $\vec{F} = \vec{I} + \vec{J}$. The hyperfine splitting for $l = 0$ is given as:

$$\Delta E_{hfs} = -\vec{\mu}_e \cdot \vec{B}(\vec{r}) = \frac{a}{2}[F(F+1) - 3/4 - I(I+1)], \tag{A.23}$$

where $a = \frac{8}{3} g_N \frac{m}{M_N} (Z\alpha)^4 mc^2 \frac{1}{n^3}$, and g_N is the gyromagnetic ratio of the nucleus and Z is the nuclear charge. The simple case of a for the proton is given in Eq. A.21.

A.3 Hydrogen atom in the magnetic field: the Zeeman effect

When considering the Zeeman effect, it is easier first to consider the hydrogen atom without hyperfine structure. In the presence of an external magnetic field, these different states will have different energies due to the different orientations of the magnetic dipoles in the external field. The splitting of these energy levels is called the Zeeman effect.

The Hamiltonian of the Zeeman effect is:

$$\Delta H_z = -\vec{\mu}_e \cdot \vec{\mathrm{B}},$$

where $\vec{\mu_e}$ is the total magnetic dipole moment of electron. The total magnetic dipole moment of the electron is a sum of the contributions of the orbital angular momentum $\vec{l}$ and the spin angular momentum $\vec{s}$:

$$\vec{\mu} = \vec{\mu}_l + \vec{\mu}_s = \mu_B(g_l \vec{L} + g_s \vec{S}) = -\mu_B(\vec{L} + 2\vec{S}), \tag{A.24}$$

where for the electron, $g_l = 1$, and $g_s = 2$ and μ_B is the Bohr magneton.

Because of the difference in the orbital and spin gyromagnetic ratios of the electron, $\vec{\mu}$ is in general not parallel to $\vec{J} = \vec{L} + \vec{S}$. So, as $\vec{L}$ and $\vec{S}$ precess around $\vec{J}$, the total dipole moment $\vec{\mu}$ also precesses around $\vec{J}$. Assuming the external field to be in the z-direction, this field causes $\vec{J}$ to precess around the z-axis. Typical internal magnetic fields in the hydrogen atom are of the order 1 Tesla. If the external field is much weaker than 1 Tesla, which is the case for almost all practical purposes, then the precession of $\vec{J}$ around the z-axis will take place much slower than the precession of $\vec{\mu}$ around $\vec{J}$. Therefore, it is reasonable to evaluate μ_B by first evaluating the projection of $\vec{\mu}$ on to $\vec{J}$, called μ_J, and then evaluating the projection of this onto B, thus giving some average projection of $\vec{\mu}$ on to $\vec{B}$. The projection of $\vec{\mu}$ onto $\vec{J}$ is:

$$\mu_J = \frac{\vec{\mu} \cdot \vec{J}}{|J|} = -\mu_B \frac{(\vec{L} + 2\vec{S}) \cdot (\vec{L} + \vec{S})}{|J|}. \tag{A.25}$$

Therefore,

$$\mu_H = \mu_J \frac{\vec{J}\cdot\vec{B}}{|J||B|} = \mu_J \frac{J_z}{|J|} = -\mu_B \frac{(\vec{L}+2\vec{S})\cdot(\vec{L}+\vec{S})J_z}{J^2}. \tag{A.26}$$

Evaluating the dot product using again the fact that $J^2 = L^2 + S^2 + 2\vec{L}\cdot\vec{S}$ yields:

$$\mu_H = -\mu_B \frac{3J^2 + S^2 - L^2}{2J^2} J_z \tag{A.27}$$

Analyzing the first-order perturbation theory, the energy shift becomes:

$$\Delta E_z = \mu_H B = -g\mu_B m_j B, \tag{A.28}$$

where:

$$g = 1 + \frac{j(j+1) + s(s+1) - l(l+1)}{2j(j+1)} \tag{A.29}$$

is called the Landé g factor. Note that if $s = 0$, then $j = l$ and $g = 1$, and if $l = 0$, $j = s$ and $g = 2$. The Landé g factor thus gives some effective gyromagnetic ratio for the electron when the total dipole moment originates partially from orbital the angular momentum and partially from the spin. m_j is a good quantum number, and the degeneracy of the $2j + 1$ states is removed.

It can be seen that the energy shift, caused by the Zeeman effect, is linear in B and m_j. Therefore, for a set of states with particular values of n, l, j, the individual sub-states with different m_j will be equally spaced in energy, separated by $m_j B$. However, the spacing will, in general, be different for a set of states with different n, l, j due to the difference in the Lande g factor.

B. χ^2 fitting of the polarization asymmetries

The objective of this appendix is to explain the procedure which is used to find the analyzing powers and the beam polarization using the cross-section relation, Eq. (2.56).

When one performs an experiment with a polarized beam, one option is to measure an asymmetry which is proportional to the product of the analyzing power of the reaction and the beam polarization. Knowing one of these quantities, one can determine the other. In the experiment outlined in Chapter 3, both methods were used simultaneously with two different setups.

For a purely unpolarized beam ($p_{ZZ} = 0$), the data analysis is rather simple. The analyzing powers for the reaction $^{12}\mathrm{C}(\vec{d},\alpha)^{10}\mathrm{B}(2^+)$ studied with the SMART spectrograph, are known theoretically [63, 64] at 0°. Therefore, by measuring the polarization asymmetries and by using the theoretical analyzing powers, the value of the beam-polarization is calculated for every polarization mode using Eq. 3.2. By using the extracted polarization from the SMART part, and by measuring the polarization asymmetry at the D-room setup, the analyzing powers can be calculated analytically. But for an impure off-mode ($p_{ZZ} \neq 0$), a different procedure was used.

The analytic expression 2.56, excludes asymmetries which are caused by experimental inefficiencies. For instance, an off-polarization beam can practically have a small non-zero polarization which affects the value of the up-polarization and down-polarization. This small off-polarization can be treated as a perturbation in the equations, as it is shown in equation (B.1),

$$\frac{I^{off}}{I_0} = 1 + \frac{p_{ZZ}^{off}}{4}(3\cos^2\beta - 1), \tag{B.1}$$

where I^{off}, p_{ZZ}^{off} are the cross sections and tensor polarization of the beam in the off-polarization mode, respectively, and I_0 is the unpolarized beam cross section. Since we only have off-mode measurements and not I_0, we should eliminate I_0 from our equations. By substituting equation B.1 in equation 3.2 and separating the measurable quantities for each mode on the right-hand side, we have,

$$\begin{aligned}
\frac{I^{\uparrow} - I^{off}}{I^{off}}\mu &= p_{ZZ}^{\uparrow} - p_{ZZ}^{off} + \left(\frac{p_{ZZ}^{\uparrow} p_{ZZ}^{off}}{\mu}\right); \\
\frac{I^{\downarrow} - I^{off}}{I^{off}}\mu &= p_{ZZ}^{\downarrow} - p_{ZZ}^{off} + \left(\frac{p_{ZZ}^{\downarrow} p_{ZZ}^{off}}{\mu}\right),
\end{aligned} \tag{B.2}$$

where $\mu = \frac{4}{(3\cos^2\beta - 1)}$, $I^{\uparrow}, I^{\downarrow}, I^{off}$ are cross sections of the up, down, and off-polarization modes and $p_{ZZ}^{\uparrow}, p_{ZZ}^{\downarrow}, p_{ZZ}^{off}$ are up, down, and off tensor polarizations.

Equation (B.2) could be solved by measuring the $I^{\uparrow}, I^{\downarrow}, I_0$ in the SMART spectrograph.

But by including p_{ZZ}^{off} the number of unknown quantities is larger than the number of measurements. The second part of the experiment, D-room complements the first part. In the D-room, 12 cross sections are measured, $I(p_{ZZ}^{\uparrow}, p_{ZZ}^{\downarrow}, p_{ZZ}^{off})$ for four sides namely Left, Right, Up and Down. Equation (2.56) is simplified for four sides, Left($\phi = 0°$), Right($\phi = 180°$), Up($\phi = 270°$), and Down($\phi = 90°$) as Eq.B.3, where $I_0(L, R, U, D)$ are unpolarized beam cross sections for left, Right, Up, and Down and the angle β is known from a separate and dedicated measurement.

Altogether by using a χ^2 fitting from 12 measurements in the D-room $I(p_{ZZ}^{\uparrow}, p_{ZZ}^{\downarrow}, p_{ZZ}^{off})$ (L,R,U,D) and 2 measurements in the SMART, we can find 11 parameters (iT_{11},T_{20},T_{22},T_{21}, $p_{ZZ}^{\uparrow}, p_{ZZ}^{\downarrow}, p_{ZZ}^{off}$, and $I_0(L, R, U, D)$). Equations B.2, and B.3 show the measured observables in red color and the fitted observables in blue. The fitting procedure receives a set of 14 measurements as input for every run at different angles and after a χ^2 minimization, produces 11 observables with which the number of degrees of freedom is 3.

In this fitting procedure the value of β is the same for all three polarization modes. Errors are extracted from the fitting routine. These depend on the errors of measurements and the fit χ^2 for each fit.

$$
\begin{aligned}
I^{off}(R) &= I_0(R)(1-\sqrt{3}iT_{11}(\theta)p_Z^{off}\sin\beta+\frac{T_{20}(\theta)p_{ZZ}^{off}}{\sqrt{8}}(3\cos^2\beta-1)-\frac{\sqrt{3}}{2}T_{22}(\theta)p_{ZZ}^{off}\sin^2\beta),\\
I^{\uparrow}(R) &= I_0(R)(1-\sqrt{3}iT_{11}(\theta)p_Z^{\uparrow}\sin\beta+\frac{T_{20}(\theta)p_{ZZ}^{\uparrow}}{\sqrt{8}}(3\cos^2\beta-1)-\frac{\sqrt{3}}{2}T_{22}(\theta)p_{ZZ}^{\uparrow}\sin^2\beta),\\
I^{\downarrow}(R) &= I_0(R)(1-\sqrt{3}iT_{11}(\theta)p_Z^{\downarrow}\sin\beta+\frac{T_{20}(\theta)p_{ZZ}^{\downarrow}}{\sqrt{8}}(3\cos^2\beta-1)-\frac{\sqrt{3}}{2}T_{22}(\theta)p_{ZZ}^{\downarrow}\sin^2\beta),\\
I^{off}(L) &= I_0(L)(1+\sqrt{3}iT_{11}(\theta)p_Z^{off}\sin\beta+\frac{T_{20}(\theta)p_{ZZ}^{off}}{\sqrt{8}}(3\cos^2\beta-1)-\frac{\sqrt{3}}{2}T_{22}(\theta)p_{ZZ}^{off}\sin^2\beta),\\
I^{\uparrow}(L) &= I_0(L)(1+\sqrt{3}iT_{11}(\theta)p_Z^{\uparrow}\sin\beta+\frac{T_{20}(\theta)p_{ZZ}^{\uparrow}}{\sqrt{8}}(3\cos^2\beta-1)-\frac{\sqrt{3}}{2}T_{22}(\theta)p_{ZZ}^{\uparrow}\sin^2\beta),\\
I^{\downarrow}(L) &= I_0(L)(1+\sqrt{3}iT_{11}(\theta)p_Z^{\downarrow}\sin\beta+\frac{T_{20}(\theta)p_{ZZ}^{\downarrow}}{\sqrt{8}}(3\cos^2\beta-1)-\frac{\sqrt{3}}{2}T_{22}(\theta)p_{ZZ}^{\downarrow}\sin^2\beta),\\
I^{off}(D) &= I_0(D)(1+\frac{T_{20}(\theta)p_{ZZ}^{off}}{\sqrt{8}}(3\cos^2\beta-1)+\sqrt{3}T_{21}(\theta)p_{ZZ}^{off}\sin\beta\cos\beta+\frac{\sqrt{3}}{2}T_{22}(\theta)p_{ZZ}^{off}\sin^2\beta),\\
I^{\uparrow}(D) &= I_0(D)(1+\frac{T_{20}(\theta)p_{ZZ}^{\uparrow}}{\sqrt{8}}(3\cos^2\beta-1)+\sqrt{3}T_{21}(\theta)p_{ZZ}^{\uparrow}\sin\beta\cos\beta+\frac{\sqrt{3}}{2}T_{22}(\theta)p_{ZZ}^{\uparrow}\sin^2\beta),\\
I^{\downarrow}(D) &= I_0(D)(1+\frac{T_{20}(\theta)p_{ZZ}^{\downarrow}}{\sqrt{8}}(3\cos^2\beta-1)+\sqrt{3}T_{21}(\theta)p_{ZZ}^{\downarrow}\sin\beta\cos\beta+\frac{\sqrt{3}}{2}T_{22}(\theta)p_{ZZ}^{\downarrow}\sin^2\beta),\\
I^{off}(U) &= I_0(U)(1+\frac{T_{20}(\theta)p_{ZZ}^{off}}{\sqrt{8}}(3\cos^2\beta-1)-\sqrt{3}T_{21}(\theta)p_{ZZ}^{off}\sin\beta\cos\beta+\frac{\sqrt{3}}{2}T_{22}(\theta)p_{ZZ}^{off}\sin^2\beta),\\
I^{\uparrow}(U) &= I_0(U)(1+\frac{T_{20}(\theta)p_{ZZ}^{\uparrow}}{\sqrt{8}}(3\cos^2\beta-1)-\sqrt{3}T_{21}(\theta)p_{ZZ}^{\uparrow}\sin\beta\cos\beta+\frac{\sqrt{3}}{2}T_{22}(\theta)p_{ZZ}^{\uparrow}\sin^2\beta),\\
I^{\downarrow}(U) &= I_0(U)(1+\frac{T_{20}(\theta)p_{ZZ}^{\downarrow}}{\sqrt{8}}(3\cos^2\beta-1)-\sqrt{3}T_{21}(\theta)p_{ZZ}^{\downarrow}\sin\beta\cos\beta+\frac{\sqrt{3}}{2}T_{22}(\theta)p_{ZZ}^{\downarrow}\sin^2\beta).
\end{aligned}
\tag{B.3}
$$

C. The data acquisition of BINA

Figure C.1 shows the BINA-DAQ system schematically. The FERA manager receives a signal from the trigger unit, M-Gate, and generates G1 and G2 which are used to communicate with TDC-wall, ADC-wall, Long-ball, short-ball, and E1 PCOS-III modules, respectively. By exchanging the RQI/RQO with FERAs, FERA manager issues a request for data from FERAs. Now, FERAs have to write the data to memory. The WSO/WSI signals are like a hand shaking between FERAs and the memory unit. When data are transfered to the memory units, they issue acknowledgment signals, WAO/WAI, to FERAs. The process of reading the data from FERA and PCOS-III are according to the event structure of BINA. First FERAs of wall E and ΔE detectors are read; then ball long and short, followed by the TDC outputs, and finally by the PCOS-III information. Finally, the FERA manager sends a "clear" signal to all other blocks to be ready for another event.

In order to improve the data transfer rate, a ping-pong method is used to write the data to memories and on the disk. When one of two memories, e.g. Memory 1, is almost full, it issues an overflow (OVF) signal. Then, after FERA readout cycle is finished, the real-time processor receives an interrupt and prevents next triggers to be accepted. Subsequently, it disables Memory 1, enables Memory 2 and enables the next trigger. The data flow is now directed to Memory 2, while the data from Memory 1 are transfered to the external storage device. Finally, Memory 1 is cleared and ready to accept data, but it will be enabled only after Memory 2 is filled up. It helps to minimize the acquisition dead-time and increases the acquisition rate substantially.

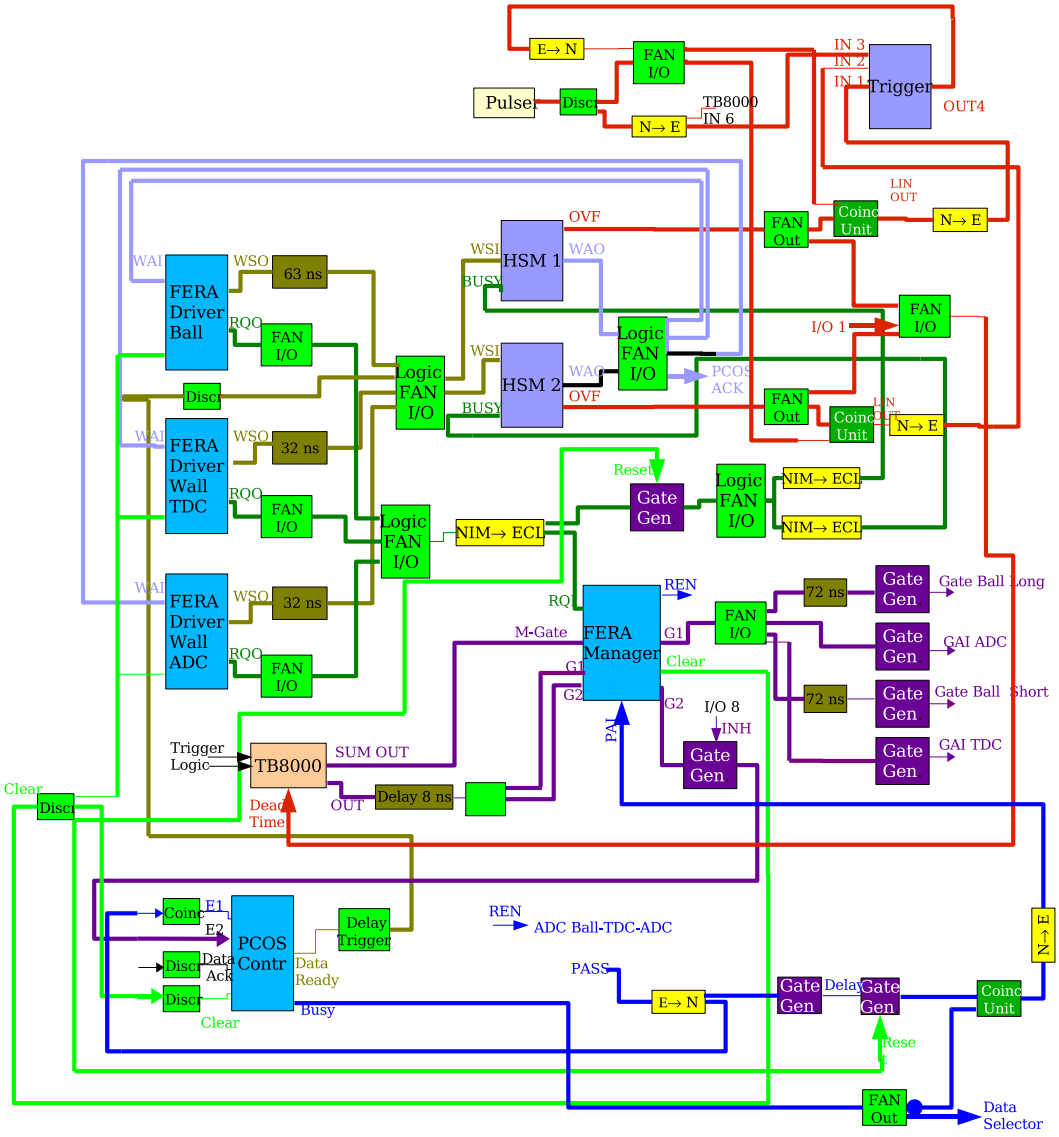

Figure C.1: A schematic overview of the individual elements in the DAQ of BINA. The communication between the different units are indicated.

D. The trigger unit of BINA

The trigger unit is composed of logical units which combine information from backward ball, forward-wall E, and ΔE. Figure D.1 shows the logical units that are used in the trigger conditions.

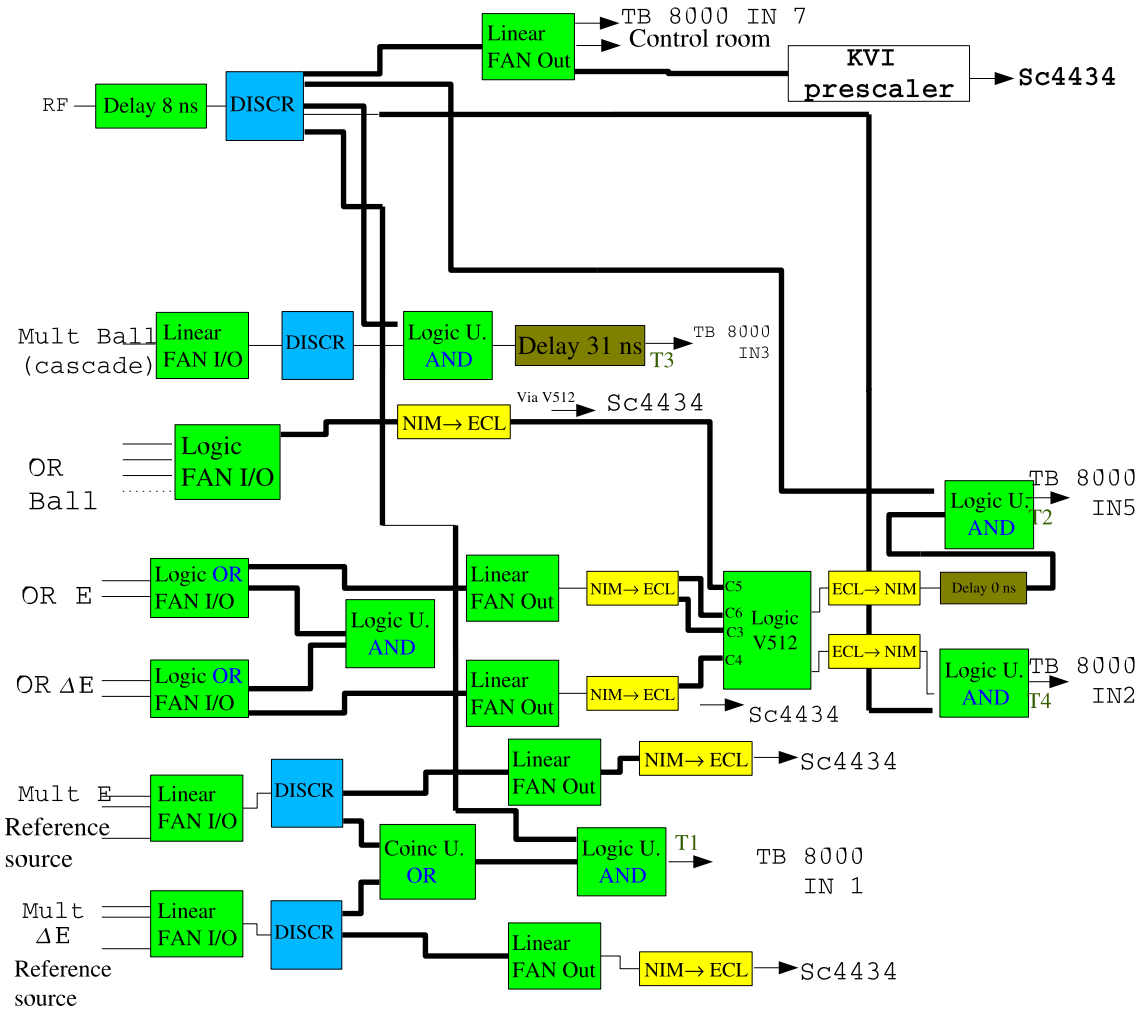

Figure D.1: The trigger units receive signals from the Wall-E/ΔE and Ball and prepares logical gates to be used by FERA-manager.

E. The event structure of BINA

There are two types of events in the experiments with BINA: normal events which carry information about the reaction for every event, and scaler events which have a summary of information about the events within the last second including some useful information such as, the value of beam current, time stamp, etc..

The event structure of a normal event in the BINA experiments is shown as blocks in Fig. E.1. The header block contains key information about the event such as: number

Figure E.1: Structure of a real event buffer in the BINA experiments given as blocks.

of the following words, event ID (normal and scaler), and the beam polarization. Next blocks have practical information about the firing channels and value of the saved charges in every channel. Ball-long and Ball-short and Wall-E and ΔE contain information about the ADC signals from the ball and the wall, respectively. The TDC blocks contain TDC information from the Wall-E and ΔE detectors. Also, part of the TDC block is devoted to the trigger information.

During the experiment, normal events are constructed with every event according to the block-diagram which is shown in Fig. E.1 and are sent to the disk. However, scaler events are built every second. Figure E.2 shows the structure of a scaler event as block diagrams. The scaler event contains the count rate of every single detector during the

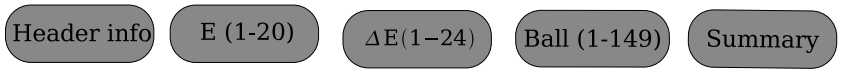

Figure E.2: Structure of a scaler event in the experiments with BINA as blocks.

last second and also the statistical information about the trigger conditions such as count rates in the forward-wall and backward-ball, number of the accepted and rejected events, calculating the count rates before and after prescaler and dead-time, and so on.

In the following, a sample normal and scaler events are explained in details.

E.1 Analysis of a sample normal event in the experiments with BINA

The general structure of a normal event in the experiment with BINA is shown as blocks in Fig. E.1. In this section we analyze one of the prototype events where all detectors were firing and it has the maximum size. Figure E.3 shows details of a real event. To interpret

one of the events, the first three numbers are very important. They are called the event header. The first number presents the number of data words that exists in this event buffer, 018f(Hex) = 399 (dec). The second number is the event type (1 for normal events, 2 for scaler events). The third number is the beam polarization, 0 means a Hexapole-Off beam. From the forth number, we have information from FERAs and they carry real information about the ADCs. Fourth number is the first data word from FERA and it is a header word. Structure of the normal and header FERA words are given in Fig. E.4. One of the header words in Fig. E.3 is translated according to the scheme shown in Fig. E.4. For instance, number 20:8002 should be translated from hexadecimal to binomial base.

$$20 : 8002(\mathrm{HEX}) = 1, 0000, 000, 0000, 0010(\mathrm{bin}). \tag{E.1}$$

This header word indicates that, 16 data words are following it. The virtual station number,VSN, is two (2) which is uniquely defined for each module on the CAMAC crate. Therefore, this header word tells us from which module it comes and how many data words are following it. The following numbers are the real QDC charges for each channel. For example in this buffer, 29:404a means,

$$29 : 404a(HEX) = 0, 1000, 0000, 1001, 010(bin). \tag{E.2}$$

Referring to Fig. E.4 reading from left, first bit is 0 to show that it is a data word, the second 4 numbers are (8 dec) and it represents the channel number and the last 11 bits show the value of energy (74 dec). After FERA buffer from first crate, the FERA buffer from second crate (8022, 8023 and 8024) and also TDC buffers (8140, 8141 and 8142) are indicated. The structure of buffers from TDC is the same as ADC buffers. The word number 397:ffff, marks the end of the events from ADC and TDC. Buffers after this tag are coming from PCOS.

E.2 Analysis of a scaler event in the experiments with BINA.

The structure of a scaler event in the experiments with BINA is shown as blocks in Fig. E.2. The header block is explained in the previous section. The E(1-20), ΔE (1-24), ball (1-149) are the count rates for every detector in the system which is read out by scaler modules[1]. The last block, Summary, carries the statistical information about the triggers. The information inside the Summary block is given in Table E.1. In this table, channels 0-4 show the original rates of T1, T2, the reference 10 kHz, RF divided by 10^6, and the beam Current as read out from the Faraday Cup. Channels 5-9 show the same quantities after dead-time corrections, and channels 10-14 are the same but after dead-time and prescaling. The second column can be used as the complementary information to the first column. The OR E, OR ΔE, OR WALL, and OR BALL are used already to extract the trigger tag for every event. The 10 kHz and 10 kHz AND DT are used for the dead-time calculations. Finally, the bits from 28 to 31 are the accumulated accepted and rejected events by the data-acquisition.

[1] CAEN: Mod.V830

Event 15400:
0:18f , 1:1 , 2:0 , 3:8001, 4:2f , 5:83e , 6:102f, 7:182b,
8:2020, 9:2834, 10:302b, 11:382a, 12:4026, 13:481c, 14:502f, 15:5823,
16:6028, 17:681d, 18:703c, 19:7835, 20:8002, 21:47 , 22:878 , 23:103a,
24:1841, 25:2041, 26:2849, 27:3043, 28:383c, 29:404a, 30:4846, 31:504b,
32:5838, 33:604f, 34:6860, 35:7044, 36:7858, 37:8003, 38:32 , 39:823 ,
40:1022, 41:1839, 42:202b, 43:2822, 44:3024, 45:3825, 46:402f, 47:4824,
48:5041, 49:5829, 50:6023, 51:682c, 52:703a, 53:7827, 54:8004, 55:1e ,
56:826 , 57:1022, 58:1834, 59:2022, 60:2870, 61:302b, 62:382e, 63:402a,
64:4831, 65:5031, 66:5826, 67:6030, 68:6828, 69:702f, 70:7823, 71:8005,
72:16 , 73:82f , 74:1020, 75:181d, 76:2031, 77:2835, 78:303d, 79:3829,
80:4032, 81:482c, 82:5032, 83:582b, 84:6053, 85:6838, 86:702e, 87:7854,
88:8006, 89:2c , 90:820 , 91:1031, 92:1828, 93:202f, 94:2831, 95:3030,
96:3826, 97:4011, 98:480f, 99:5026, 100:582a, 101:602a, 102:683e, 103:7019,
104:7836, 105:8007, 106:1c , 107:81e , 108:1001, 109:1830, 110:201c, 111:2830,
112:3017, 113:380f, 114:4017, 115:482b, 116:5024, 117:583a, 118:6018, 119:6819,
120:701f, 121:782d, 122:f808, 123:34 , 124:826 , 125:1028, 126:1820, 127:2028,
128:282a, 129:3046, 130:3810, 131:4027, 132:4824, 133:5024, 134:582a, 135:6819,
136:7028, 137:782c, 138:f809, 139:29 , 140:81c , 141:102d, 142:1827, 143:2014,
144:282d, 145:3025, 146:3826, 147:4021, 148:4817, 149:5024, 150:5824, 151:6003,
152:680f, 153:781d, 154:f80a, 155:7a , 156:81a , 157:103c, 158:1839, 159:2044,
160:2821, 161:3056, 162:382f, 163:402c, 164:4833, 165:502c, 166:583f, 167:60a4,
168:6831, 169:7021, 170:800b, 171:3c , 172:839 , 173:1034, 174:181e, 175:2036,
176:2835, 177:3020, 178:3841, 179:4003, 180:4837, 181:5040, 182:583a, 183:603d,
184:6821, 185:7037, 186:7846, 187:800c, 188:47 , 189:83d , 190:1041, 191:183d,
192:2049, 193:2838, 194:303f, 195:3835, 196:4047, 197:4842, 198:503e, 199:583a,
200:6042, 201:6845, 202:7040, 203:783f, 204:800d, 205:3c , 206:837 , 207:1037,
208:1832, 209:203b, 210:2839, 211:303c, 212:3838, 213:403f, 214:4836, 215:503f,
216:583a, 217:6043, 218:6844, 219:7043, 220:7838, 221:800e, 222:36 , 223:839 ,
224:103b, 225:1835, 226:2035, 227:283a, 228:302d, 229:383a, 230:4037, 231:4838,
232:5038, 233:5828, 234:6038, 235:6839, 236:703b, 237:7836, 238:800f, 239:39 ,
240:83a , 241:103d, 242:1841, 243:2042, 244:2839, 245:302f, 246:3837, 247:4037,
248:483a, 249:502c, 250:5839, 251:603d, 252:6843, 253:7040, 254:7837, 255:8010,
256:2e , 257:82d , 258:1030, 259:182f, 260:2039, 261:2833, 262:3030, 263:382f,
264:4035, 265:482f, 266:5030, 267:582a, 268:6033, 269:6830, 270:7033, 271:782c,
272:8011, 273:2a , 274:828 , 275:1026, 276:1822, 277:2033, 278:2824, 279:302d,
280:382a, 281:402e, 282:4827, 283:502d, 284:582a, 285:602b, 286:6830, 287:7026,
288:782b, 289:8012, 290:3b , 291:838 , 292:103f, 293:1835, 294:203a, 295:2835,
296:3041, 297:382c, 298:4037, 299:482c, 300:503f, 301:5831, 302:6030, 303:6832,
304:702c, 305:7834, 306:8013, 307:3c , 308:83d , 309:1042, 310:183e, 311:2044,
312:283e, 313:303e, 314:383d, 315:4044, 316:4840, 317:504a, 318:5840, 319:603f,
320:6841, 321:703f, 322:783d, 323:8022, 324:1a , 325:815 , 326:1015, 327:1818,
328:2013, 329:2809, 330:3019, 331:3813, 332:4018, 333:4814, 334:501b, 335:5818,
336:601c, 337:6825, 338:7014, 339:780e, 340:8023, 341:1c , 342:814 , 343:101a,
344:1818, 345:201c, 346:2819, 347:301c, 348:3814, 349:401b, 350:4817, 351:5019,
352:581c, 353:601e, 354:6818, 355:7012, 356:7813, 357:8024, 358:13 , 359:814 ,
360:1015, 361:1810, 362:2014, 363:2811, 364:3016, 365:380c, 366:401a, 367:480e,
368:5017, 369:580c, 370:6010, 371:6812, 372:7010, 373:7812, 374:8140, 375:5d ,
376:95 , 377:1a2 , 378:206 , 379:227 , 380:236 , 381:2639, 382:2649, 383:26c0,
384:26d1, 385:26e1, 386:26f3, 387:282f, 388:2873, 389:8141, 390:4809, 391:481a,
392:482b, 393:483c, 394:484c, 395:485d, 396:8142, 397:ffff, 398:c400,

Figure E.3: Information inside an event. The first three numbers are the event header. From 4^{th} number to 397:ffff are events from FERA and after this tag, PCOS-III events are placed.

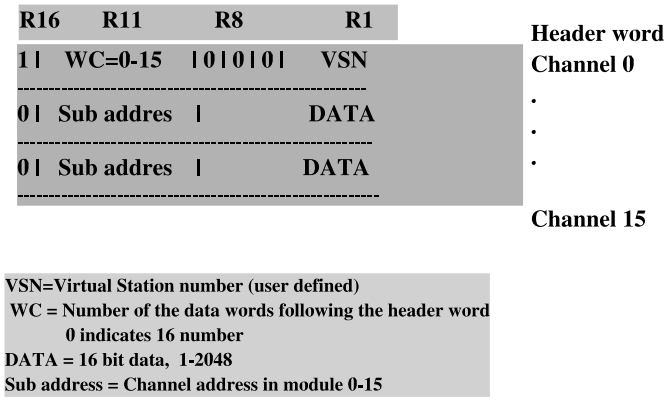

Figure E.4: The structure of normal word and header word in FERA events.

Table E.1: Information inside the summary block of the scaler event. More details are explained in the text.

Chan	Quantity	Chan	Quantity
0	T1	16	OR E
1	T2	17	OR ΔE
2	10 kHz	18	OR WALL
3	RF/10^6	19	OR BALL
4	FC	20	T1
5	T1 AND DT	21	T2
6	T2 AND DT	22	10 kHz
7	10 kHz AND DT	23	10 kHz AND DT
8	RF/10^6 AND DT	24	empty
9	FC AND DT	25	# E
10	T1 AND DT AND Pr	26	# ΔE
11	T2 AND DT AND Pr	27	empty
12	10 kHz AND DT AND Pr	28	Total FERA
13	RF/10^6 AND DT AND Pr	29	Accepted FERA
14	FC AND DT AND Pr	30	Rejected FERA
15	empty	31	Tout

F. Extracting the Cross Sections

A general form for the differential cross section is

$$\frac{d\sigma}{d\Omega}\left[\frac{\text{mb}}{\text{sr}}\right] = \frac{N_{\text{out}}}{I[\text{nC}]/Z} \cdot \underbrace{\frac{1}{N[1/\text{mg}]\,\delta\text{x}[\text{mg/cm}^2]}}_{\equiv t[1/\text{mb}]} \cdot \frac{1}{\Delta\Omega[\text{sr}]}, \tag{F.1}$$

where N_{out} is the number of outgoing particles, I is the total integrated charge in nC, Z is the charge per projectile, δx is the target thickness in mg/cm^2, N is the number of scattering centers per mg of the target and $\Delta\Omega$ is the solid angle in sr.

The target thickness is obtained from

$$t[1/\text{mb}] = \delta\text{x}[\text{mg/cm}^2] \cdot \frac{n_{\text{atoms}}}{m^{\text{mol}}_{\text{target}}[\text{u}]} \cdot N_A \cdot 10^{-3} \cdot 10^{-27}\left[\frac{\text{cm}^2}{\text{mb}}\right],$$

where N_A is Avogadro's number, n_{atoms} is the number of atoms per compound molecule, and $m^{\text{mol}}_{\text{target}}(\text{u})$ is the target weight in atomic units, with $1u = 10^3\text{mg}/1\text{mol}$.

$$\begin{aligned}\frac{1}{e} \cdot 10^{-9} \cdot \underbrace{10^{-3} \cdot N_A \cdot 10^{-27}}_{N\delta\text{x}[\text{cm}^2/(\text{mb}\cdot\text{mol})]} \cdot \underbrace{10^{-3}}_{\Delta\Omega} &= \frac{N_A}{e} \cdot 10^{-42}\left[\frac{\text{cm}^2}{\text{mb}\cdot\text{C}\cdot\text{mol}}\right] \\ &\approx 3.75872\left[\frac{\text{cm}^2}{\text{mb}\cdot\text{C}\cdot\text{mol}}\right]\end{aligned} \tag{F.2}$$

where e is the elementary charge. Inserting these relations into (F.1) leads to the formula used during this work to calculate the cross sections:

$$\frac{d\sigma}{d\Omega}\left[\frac{\text{mb}}{\text{sr}}\right] = \frac{e}{N_A} \cdot 10^{42} \cdot \frac{N_{\text{out}}}{I[\text{nC}]/Z} \cdot \left(\delta\text{x}[\text{mg/cm}^2] \cdot \frac{n_{\text{atoms}}}{m^{\text{mol}}_{\text{target}}[\text{u}]}\right)^{-1} \cdot \frac{1}{\Delta\Omega[\text{msr}]} \tag{F.3}$$

For scattering of protons, $Z = 1$, on deuterons using a liquid deuterium target during the experiments in this work, $n_{\text{atoms}} = 2$ and $m^{\text{mol}}_{\text{target}}(\text{u}) = 4.028$ and equation (F.3) results in:

$$\frac{d\sigma}{d\Omega}\left[\frac{\text{mb}}{\text{sr}}\right] = \frac{1}{3.75872} \cdot \frac{N_{\text{out}}}{I[\text{nC}]} \cdot \left(\frac{1}{\delta\text{x}[\text{mg/cm}^2] \cdot 0.496}\right) \cdot \frac{1}{\Delta\Omega[\text{msr}]}.$$